AFRL-RX-WP-JA-2015-0130

MECHANICAL PROPERTIES OF LOW-DENSITY, REFRACTORY MULTI-PRINCIPAL ELEMENT ALLOYS OF THE Cr–Nb–Ti–V–Zr SYSTEM (POSTPRINT)

O.N. Senkov, S.V. Senkova, D.B. Miracle, and C. Woodward
AFRL/RXCM

APRIL 2014
Interim Report

AIR FORCE RESEARCH LABORATORY
MATERIALS AND MANUFACTURING DIRECTORATE
WRIGHT-PATTERSON AIR FORCE BASE OH 45433-7750
AIR FORCE MATERIEL COMMAND
UNITED STATES AIR FORCE

NOTICE AND SIGNATURE PAGE

Using Government drawings, specifications, or other data included in this document for any purpose other than Government procurement does not in any way obligate the U.S. Government. The fact that the Government formulated or supplied the drawings, specifications, or other data does not license the holder or any other person or corporation; or convey any rights or permission to manufacture, use, or sell any patented invention that may relate to them.

Qualified requestors may obtain copies of this report from the Defense Technical Information Center (DTIC) (http://www.dtic.mil).

AFRL-RX-WP-JA-2015-0130 HAS BEEN REVIEWED AND IS APPROVED FOR PUBLICATION IN ACCORDANCE WITH ASSIGNED DISTRIBUTION STATEMENT.

//Signature//

MICHEAL E. BURBA, Project Engineer
Metals Branch
Structural Materials Division

//Signature//

DANIEL J. EVANS, Chief
Metals Branch
Structural Materials Division

//Signature//

ROBERT T. MARSHALL, Deputy Chief
Structural Materials Division
Materials And Manufacturing Directorate

This report is published in the interest of scientific and technical information exchange and its publication does not constitute the Government's approval or disapproval of its ideas or findings.

REPORT DOCUMENTATION PAGE

Form Approved
OMB No. 0704-0188

1. REPORT DATE *(DD-MM-YY)*	2. REPORT TYPE	3. DATES COVERED *(From - To)*
April 2014	Interim	19 March 2014 – 31 March 2014

4. TITLE AND SUBTITLE
MECHANICAL PROPERTIES OF LOW-DENSITY, REFRACTORY MULTI-PRINCIPAL ELEMENT ALLOYS OF THE Cr–Nb–Ti–V–Zr SYSTEM (POSTPRINT)

5a. CONTRACT NUMBER
In-house

5b. GRANT NUMBER

5c. PROGRAM ELEMENT NUMBER
62102F

6. AUTHOR(S)
O.N. Senkov, S.V. Senkova, D.B. Miracle, and C. Woodward

5d. PROJECT NUMBER
4349

5e. TASK NUMBER

5f. WORK UNIT NUMBER
X0W6

7. PERFORMING ORGANIZATION NAME(S) AND ADDRESS(ES)

AFRL/RXCM
2941 Hobson Way
Bldg 654, Rm 136
Wright-Patterson AFB, OH 45433

UES, Inc.
4401 Dayton-Xenia Rd.
Dayton, OH 45432-1894

8. PERFORMING ORGANIZATION REPORT NUMBER

9. SPONSORING/MONITORING AGENCY NAME(S) AND ADDRESS(ES)

Air Force Research Laboratory
Materials and Manufacturing Directorate
Wright-Patterson Air Force Base, OH 45433-7750
Air Force Materiel Command
United States Air Force

10. SPONSORING/MONITORING AGENCY ACRONYM(S)
AFRL/RXCM

11. SPONSORING/MONITORING AGENCY REPORT NUMBER(S)
AFRL-RX-WP-JA-2015-0130

12. DISTRIBUTION/AVAILABILITY STATEMENT
Distribution Statement A. Approved for public release; distribution unlimited.

13. SUPPLEMENTARY NOTES
Journal article published in *Materials Science & Engineering A* 565 (2013) 51-62. This report contains color. The final publication is available at http://dx.doi.org/10.1016/j msea.2012.12.018.

14. ABSTRACT

Room temperature and elevated temperature mechanical properties of four multi-principal element alloys, NbTiVZr, $NbTiV_2Zr$, CrNbTiZr and CrNbTiVZr, are reported. The alloys were prepared by vacuum arc melting followed by hot isostatic pressing and homogenization. Disordered BCC solid solution phases are the major phases in these alloys. The Cr-containing alloys additionally contain an ordered FCC Laves phase. The NbTiVZr and $NbTiV_2Zr$ alloys showed good compressive ductility at all studied temperatures while the Cr-containing alloys showed brittle-to-ductile transition occurring somewhere between 298 and 873 K. Strong work hardening was observed in the NbTiVZr and $NbTiV_2Zr$ alloys during deformation at room temperature. The alloys had yield strengths of 1105 MPa and 918 MPa, respectively, and their strength continuously increased, exceeding 2000 MPa after ~40% compression strain. The CrNbTiZr and CrNbTiVZr alloys showed high yield strength (1260 MPa and 1298 MPa, respectively) but low ductility (6% and 3% compression strain) at room temperature. Strain softening and steady state flow were typical during compression deformation of these alloys at temperatures above 873 K. In these conditions, the alloys survived 50% compression strain without fracture and their yield strength continuously decreased with an increase in temperature. During deformation at 1273 K, the NbTiVZr, $NbTiV_2Zr$, CrNbTIZr, and CrNbTiVZr alloys showed yield strengths of 58 MPa, 72 MPa, 115 MPa and 259 MPa, respectively.

15. SUBJECT TERMS
refractory alloys, crystal structure, microstructure, mechanical properties

16. SECURITY CLASSIFICATION OF:			17. LIMITATION OF ABSTRACT:	18. NUMBER OF PAGES	19a. NAME OF RESPONSIBLE PERSON (Monitor)
a. REPORT	b. ABSTRACT	c. THIS PAGE			Micheal E. Burba
Unclassified	Unclassified	Unclassified	SAR	15	19b. TELEPHONE NUMBER *(Include Area Code)* (937) 255-9795

Materials Science & Engineering A 565 (2013) 51–62

Contents lists available at SciVerse ScienceDirect

Materials Science & Engineering A

journal homepage: www.elsevier.com/locate/msea

Mechanical properties of low-density, refractory multi-principal element alloys of the Cr–Nb–Ti–V–Zr system

O.N. Senkov*, S.V. Senkova, D.B. Miracle, C. Woodward

Air Force Research Laboratory, Materials and Manufacturing Directorate, Wright-Patterson AFB, OH 45433, USA

ARTICLE INFO

Article history:
Received 21 September 2012
Received in revised form
20 November 2012
Accepted 6 December 2012
Available online 13 December 2012

Keywords:
Refractory alloys
Crystal structure
Microstructure
Mechanical properties

ABSTRACT

Room temperature and elevated temperature mechanical properties of four multi principal element alloys, NbTiVZr, $NbTiV_2Zr$, CrNbTiZr and CrNbTiVZr, are reported. The alloys were prepared by vacuum arc melting followed by hot isostatic pressing and homogenization. Disordered BCC solid solution phases are the major phases in these alloys. The Cr containing alloys additionally contain an ordered FCC Laves phase. The NbTiVZr and $NbTiV_2Zr$ alloys showed good compressive ductility at all studied temperatures while the Cr containing alloys showed brittle to ductile transition occurring somewhere between 298 and 873 K. Strong work hardening was observed in the NbTiVZr and $NbTiV_2Zr$ alloys during deformation at room temperature. The alloys had yield strengths of 1105 MPa and 918 MPa, respectively, and their strength continuously increased, exceeding 2000 MPa after ~40% compression strain. The CrNbTiZr and CrNbTiVZr alloys showed high yield strength (1260 MPa and 1298 MPa, respectively) but low ductility (6% and 3% compression strain) at room temperature. Strain softening and steady state flow were typical during compression deformation of these alloys at temperatures above 873 K. In these conditions, the alloys survived 50% compression strain without fracture and their yield strength continuously decreased with an increase in temperature. During deformation at 1273 K, the NbTiVZr, $NbTiV_2Zr$, CrNbTIZr, and CrNbTiVZr alloys showed yield strengths of 58 MPa, 72 MPa, 115 MPa and 259 MPa, respectively.

1. Introduction

Aerospace and aircraft industries demand new metallic alloys for high temperature load bearing structures and thermal protection systems. These alloys should have a balance of high temperature properties, including reduced density, superior to existing Ni base superalloys or refractory alloys. Recently a high entropy alloying approach proposed by Yeh et al. [1 3] has been applied to produce several new refractory alloys with promising combinations of room temperature and elevated temperature mechanical properties and oxidation resistance [4 9]. These are MoNbTaW, MoNbTaVW, [4,5], HfNbTaTiZr [6,7], and $CrMo_{0.5}NbTa_{0.5}TiZr$ [8,9]. The first three alloys are single phase with a BCC crystal structure, probably due to high entropy of mixing and similar atomic radii of the alloying elements. The last alloy, which includes the addition of Cr, forms an additional minor Laves phase with the FCC crystal structure [8]. The design strategies used to predict stable high entropy alloys suggest [10,11] that this is the result of adding an element, Cr, which has a much smaller atomic radius than the other alloying elements. These refractory alloys have rather high densities, in the range from 8.2 g/cm^3 for the $CrMo_{0.5}NbTa_{0.5}TiZr$ alloy to 13.8 g/cm^3 for the MoNbTaW alloy.

New refractory high entropy alloys (HEAs) with densities below 7.0 g/cm^3 have recently been produced by alloying Nb (ρ_{Nb}=8.57 g/cm^3) with four low density refractory elements, V (ρ_V=6.11 g/cm^3), Zr (ρ_{Zr}=6.51 g/cm^3), Cr (ρ_{Cr}=7.14 g/cm^3), and Ti (ρ_{Ti}=4.51 g/cm^3) at near equiatomic concentrations. The microstructures and phase compositions of these alloys have been reported elsewhere [12]. These are NbTiVZr, $NbTiV_2Zr$, CrNbTiZr, and CrNbTiVZr alloys, which have the densities of 6.52 g/cm^3, 6.34 g/cm^3, 6.67 g/cm^3, and 6.57 g/cm^3, respectively. The NbTiVZr alloy consists of a disordered body centered cubic (BCC) matrix (the volume fraction is ~95%) and sub micron sized particles of a second phase precipitated along dislocations and subgrain boundaries. The $NbTiV_2Zr$ alloy consists of a mixture of three disordered BCC phases, with volume fractions of ~52%, 28%, and 20%, respectively. The CrNbTiZr and CrNbTiVZr alloys consist of a disordered BCC phase and ordered FCC Laves phase, with the volume fraction of the latter of 35% and 61%, respectively.

The aim of the present work was to study the deformation behavior of these low density refractory alloys in a wide tem perature range and compare the properties of these alloys with the properties of other high entropy alloys and Ni superalloys.

* Corresponding author. Tel.: +1 937 255 4064.
E-mail address: oleg.senkov@wpafb.af.mil (O.N. Senkov).

0921-5093/$ - see front matter © 2012 Elsevier B.V. All rights reserved.
http://dx.doi.org/10.1016/j.msea.2012.12.018

2. Experimental procedures

The Cr Nb Ti V Zr alloys were prepared by vacuum arc melting of the nominal mixtures of the corresponding elements, hot isostatically pressed (HIPd) at 1473 K and 207 MPa for 2 h and then annealed at 1473 K for 24 h in a high purity argon. The processing details are reported in [12]. The alloy compositions are given in Table 1.

Rectangular cuboid specimens for compression testing were electric discharge machined from the homogenized alloys. The specimen compression axis was perpendicular to the alloy surface, which was in contact with the copper plate during arc melting. The specimen surfaces were mechanically polished while maintaining parallel compression faces. During high temperature testing these faces were lubricated with boron nitride. The specimen's dimensions were ~4.7 mm × 4.7 mm × 7.7 mm. Compression tests were conducted at 298 K, 873 K, 1073 K and 1273 K in a computer controlled Instron (Instron, Norwood, MA) mechanical testing machine outfitted with a Brew vacuum furnace and silicon carbide dies. Prior to each test, the furnace chamber was evacuated to ~10^{-4} N/m^2. The test specimen was then heated to the test temperature at a heating rate of ~20 K/min, soaked at the test temperature for 15 min under 5 N controlled load, and then compressed to a 50% height reduction or to fracture, whichever happened first. A constant ramp speed that corresponded to an initial strain rate of 10^{-3} s^{-1} was used. Room temperature tests were conducted at the same strain rate conditions in air, using a servo hydraulic MTS testing machine, and thin Teflon foil was used between the compression faces and silicon carbide dies to reduce friction. The deformation of all specimens was video recorded and image correlation software Vic Gauge (Correlated Solutions, Inc.) was used to measure strains.

Vickers microhardness was measured on the polished cross section surfaces of non deformed and deformed specimens using a 136° Vickers diamond pyramid under 500 g load applied for 20 s. The microstructure was analyzed with the use of a scanning electron microscope (SEM) Quanta 600F (FEI, North America NanoPort, Hillsboro, Oregon, USA) equipped with a backscatter electron (BSE), energy dispersive X ray spectroscopy (EDS), and electron backscatter diffraction (EBSD) detectors.

Table 1
Chemical compositions (in at%) and density, ρ of the alloys studied in this work.

Alloy	Cr	Nb	Ti	V	Zr	ρ (g/cm^3)
NbTiVZr	–	28.3	24.5	23.0	24.2	6.52
NbTiV$_2$Zr	–	22.6	19.4	37.2	20.8	6.34
CrNbTiZr	24.6	26.7	23.9	–	24.8	6.67
CrNbTiVZr	20.2	20.0	19.9	19.6	20.3	6.57

3. Results

3.1. Compression properties

The engineering stress vs. engineering strain curves of the studied alloys at T=298 K, 873 K, 1073 K and 1273 K are given in Fig. 1 and the typical properties of the alloys are given in Table 2. During compression testing at room temperature (RT, 298 K), the NbTiVZr and NbTiV$_2$Zr alloys showed plastic yielding at $\sigma_{0.2}$ = 1105 MPa and 918 MPa, respectively, after which a continuous increase in their strengths occurred with an increase in the compression strain (Fig. 1a and Fig. 1b). For example, the strengths of the NbTiVZr and NbTiV$_2$Zr alloys increased to σ_{20}=1732 MPa and 1635 MPa, respectively, after compression by 20% at RT. No macroscopic fracture was observed in these alloys after 50% compression strain. The RT compression behavior of CrNbTiZr and CrNbTiVZr alloys (Fig. 1c and Fig. 1d) was different from that described above. The samples showed plastic

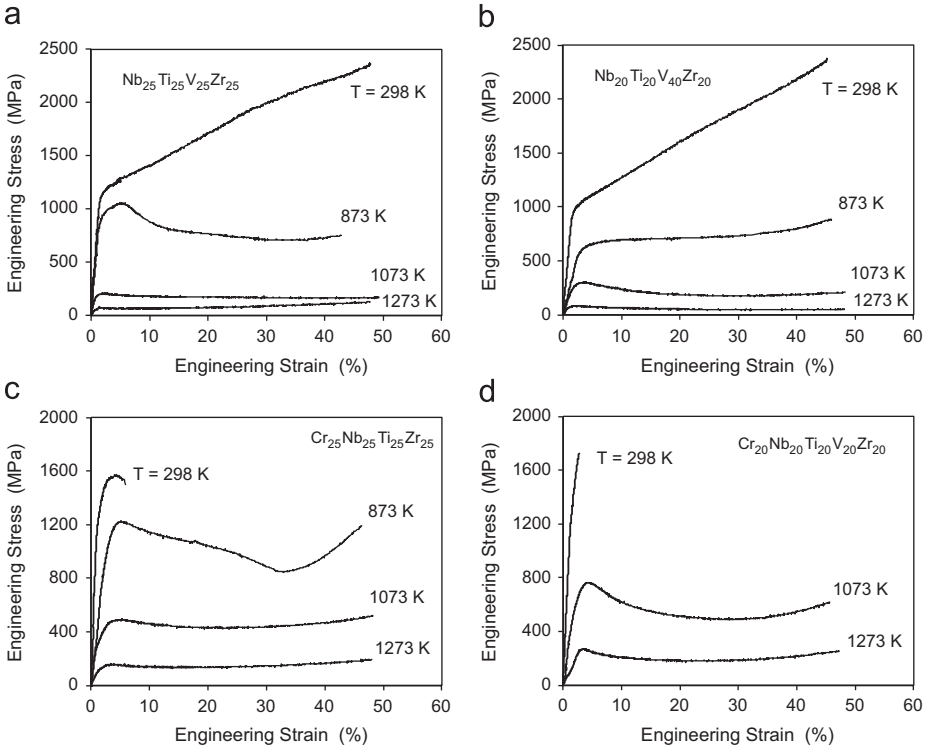

Fig. 1. Engineering stress vs. engineering strain curves of (a) NbTiVZr, (b) NbTiV$_2$Zr, (c) CrNbTiZr and (d) CrNbTiVZr alloy samples deformed by compression at T 298 K, 873 K, 1073 K and 1273 K. The strain rate is $\dot{\varepsilon}$ 10^{-3} s^{-1}.

Table 2
Compression yield stress, $\sigma_{0.2}$, flow stress at ε 10%, σ_{10}, and ε 20%, σ_{20}, and fracture strain, ε_f, of the studied alloys at different temperatures.

Alloy/properties		NbTiVZr	$NbTiV_2Zr$	CrNbTiZr	CrNbTiVZr
T 298 K	$\sigma_{0.2}$ (MPa)	1105	918	1260	1298
	σ_{10} (MPa)	1430	1300	–	–
	σ_{20} (MPa)	1732	1635	–	–
	ε_f (%)	> 50	> 50	6	3
T 873 K	$\sigma_{0.2}$ (MPa)	834	571	1035	1230
	σ_{10} (MPa)	884	701	1130	1360
	σ_{20} (MPa)	767	716	1030	–
	ε_f (%)	> 50	> 50	> 50	> 10
T 1073 K	$\sigma_{0.2}$ (MPa)	187	240	300	615
	σ_{10} (MPa)	178	228	455	601
	σ_{20} (MPa)	174	185	435	512
	ε_f (%)	> 50	> 50	> 50	> 50
T 1273 K	$\sigma_{0.2}$ (MPa)	58	72	115	259
	σ_{10} (MPa)	68	60	138	205
	σ_{20} (MPa)	77	53	136	183
	ε_f (%)	> 50	> 50	> 50	> 50

yielding at $\sigma_{0.2}$ =1260 MPa and 1298 MPa, respectively. During deformation, the CrNbTiZr alloy achieved the maximum strength, σ_m, of 1575 MPa at the engineering strain ε=4.0% and fractured by splitting and fragmentation at ε_f=6% and σ_f=1500 MPa (Fig. 1c). Here ε_f and σ_f are the engineering strain and stress at which fracture occurred. The CrNbTiVZr alloy fractured by shattering into many small pieces after approaching the maximum strength $\sigma_f=\sigma_m$=1725 MPa at ε_f=3%. The RT compression modulus, E_{comp}, of NbTiVZr, $NbTiV_2Zr$, CrNbTiZr, and CrNbTiVZr, determined with ~10% accuracy, was 80 GPa, 98 GPa, 120 GPa and 100 GPa, respectively.

With an increase in the deformation temperature, the yield stress of the alloys continuously decreases and a softening stage, during which the flow stress decreases with an increase in the plastic strain, is observed on the respective deformation curves. A steady state plastic flow stage, at which the engineering flow stress remains almost constant, is observed on the deformation curves at 1073 K and 1273 K (Fig. 1). The alloys are ductile at these temperatures and deform to 50% strain by compression without any evidence of macroscopic fracture. Among the studied alloys, the CrNbTiVZr alloy shows the most attractive elevated temperature properties (Table 1). In particular, at 1073 K and 1273 K it has $\sigma_{0.2}$=615 MPa and 256 MPa and the steady state flow stress, σ_{SS}=512 MPa and 183 MPa, respectively. The CrNbTiZr alloy has approximately half the strength of CrTiNbVZr at elevated temperatures: $\sigma_{0.2}$=300 MPa and 115 MPa at 1073 K and 1273 K, respectively. However, CrNbTiZr has a less severe flow softening response after yielding during high temperature deformation, and the steady state stress values for this alloy are higher than the respective yield stress values (Table 1). The strengths of the NbTiVZr and $NbTiV_2Zr$ alloys decrease rapidly above 873 K and during deformation at 1273 K, $\sigma_{0.2}$ and σ_{SS} of these alloys are in the range of 53 77 MPa. The deformation induced softening occurring during deformation at the elevated temperatures retains after the deformed samples are cooled down to room temperature. This is revealed by a slight decrease in microhardness of the deformed specimens relative to the homogenized condition (Table 3). For example, after deformation at 1273 K the microhardness of NbTiVZr decreases from 3.3 GPa to 3.0 GPa and that of CrNbTiVZr decreases from 4.7 GPa to 4.4 GPa.

3.2. Microstructure

The microstructure of the alloys before deformation has been reported previously in the literature [12]. Here we describe the microstructure of the alloys after deformation at 298 K and 1273 K.

Table 3
Microhardness of the cast alloys after HIP and homogenized annealing (H_{V1}) and after compression testing at 1273 K (H_{V2}).

Alloy	NbTiVZr	$NbTiV_2Zr$	CrNbTiZr	CrNbTiVZr
H_{V1} (MPa)	3285 ± 33	2987 ± 30	4099 ± 42	4720 ± 47
H_{V2} (MPa)	3035 ± 30	2958 ± 30	3888 ± 41	4402 ± 45

3.2.1. Microstructure after deformation at 298 K

Fig. 2 shows SEM backscatter images of a longitudinal cross section of a NbTiVZr alloy specimen compressed by 50% at room temperature. Extensive deformation induced intergranular cavities and cracks are observed at the side faces of the specimen (Fig. 2a) and are likely associated with high stress concentrations in these regions, as well as with the presence of second phase particles at grain boundaries. Deformed grains with clearly identified shear bands inside them are typical to the interior regions of the specimen (Fig. 2b). The shear bands are often localized at grain boundaries (Fig. 2c). The deformed specimen also contains microstructural features, such as Zr rich white spots and V rich dark submicron sized second phase particles at grain boundaries and inside the grains (Table 4), which are also present in the non deformed alloy [12]. After deformation, these features become elongated in directions perpendicular to the compression direction (see Fig. 2b d). The compositions of the non transformed matrix, white spots (transformed matrix) and second phase particles are given in (Table 4) and they are similar to the compositions of the respective regions in the non deformed alloy.

Fig. 3 shows SEM backscatter images of a longitudinal cross section of a $NbTiV_2Zr$ alloy specimen compressed by 50% at room temperature. A few small cracks develop at the side faces of the specimen (Fig. 3a). A magnified image of the longest crack illustrates that it has a blunt tip and no pores or secondary cracks are seen at the adjacent regions (Fig. 3b). The three disordered BCC phases presented in the alloy [12] (they can be identified in Fig. 3d by their different contrasts, i.e. bright, gray and dark) are ductile, and are elongated in the directions of the plastic flow with a smooth transition from one phase to another and no strain localization and crack formation at the interface boundaries (Fig. 3c and d). The chemical compositions of the phases are the same as in non deformed alloy and are given in Table 5.

Fig. 4 illustrates the microstructure of the fracture surface of a CrNbTiZr alloy specimen, which fractured after 6% compression strain. The presence of heavily deformed dimples indicates ductile fracture of the disordered BCC matrix, while cleaved surfaces between the dimples indicate brittle fracture of the ordered Laves phase in this alloy. The fracture surface is heavily decorated with fine (~1 μm in cross section) particles. These particles were produced during the explosion like fracture, which resulted in extensive fragmentation of the fractured regions.

Fig. 5 shows the fracture surface of a CrNbTiVZr alloy specimen, which fractured after 3% compression strain. The morphology is similar to that observed in the CrNbTiZr specimen, i.e. two types of fractures, ductile dimple fracture of the matrix and brittle, cleavage fracture of the Laves phase, are clearly identified (Fig. 5a and b). The brittle, explosive like fracture of the Laves phase resulted in phase fragmentation and formation of fine, powdered particles, which can be seen on the fracture surface. Fracture of this alloy released a large amount of elastic energy, which led to melting of several local regions of the fracture surface (Fig. 5c and d). The melting is evident from the presence

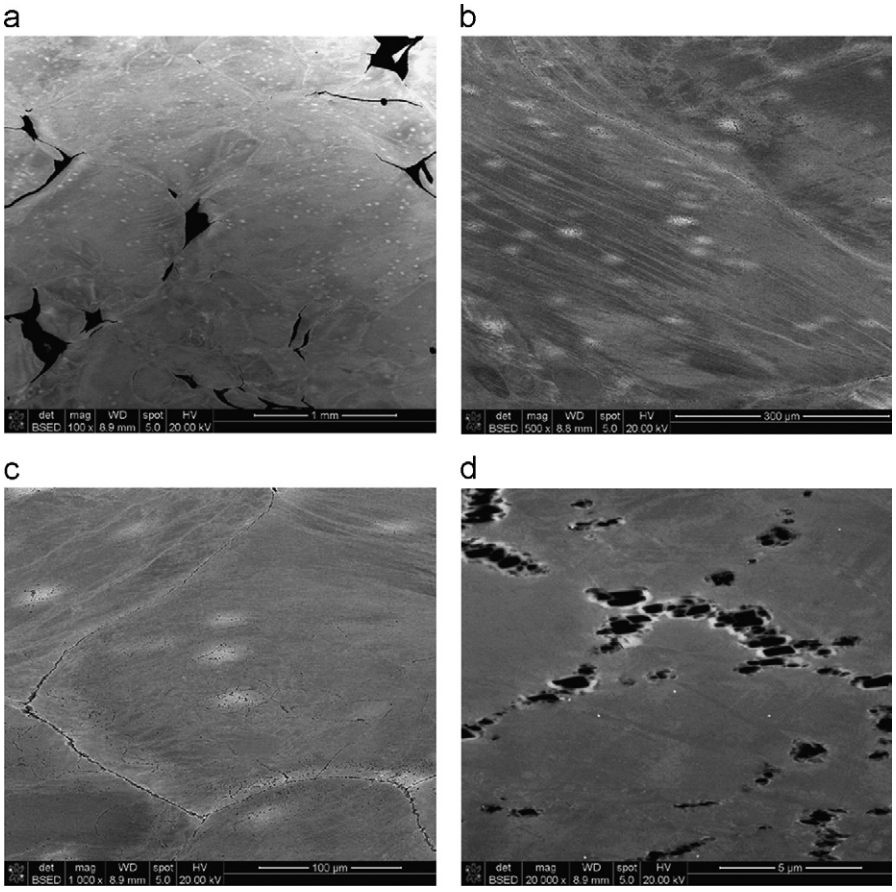

Fig. 2. The microstructure of the NbVTiZr alloy after 50% compression deformation at room temperature. (a) Cracks at grain boundaries near the sample surface; (b) elongated grain with shear bands inside it; (c) shear bands localized at grain boundaries decorated with second-phase particles; and (d) deformed (compressed) second phase particles.

Table 4
Chemical composition of the NbTiVZr alloy constituents after compression at 298 K and 1273 K.

Condition	Deformed at 298 K				Deformed at 1273 K			
At%	Nb	Ti	V	Zr	Nb	Ti	V	Zr
Non-transformed matrix (gray)	28.0	24.5	23.3	24.2	29.3	23.8	22.4	24.6
Transformed matrix (white)	24.3	23.6	20.4	31.8	24.6	23.3	11.1	41.0
Dark particles	25.3	21.1	37.8	15.8	28.5	24.8	35.0	11.7

of characteristic vein patterns and spherical particles in these regions. Melting of this type has been observed during fracture of amorphous and nano crystalline metals, and the nature of this phenomenon has been explored in the literature [13 15]. To our knowledge, it is reported here for the first time in a coarse grained alloy. It is suggested that incipient melting is due to adiabatic heating during rapid elastic energy release in the localized fracture regions.

3.2.2. *Microstructure after deformation at 1273 K*

The microstructure of the NbTiVZr alloy sample after 50% compression deformation at 1273 K is shown in Fig. 6. Some surface bulging occurs and the bottom side of the sample deforms more extensively than the top part (Fig. 6a), which is likely due to the presence of a temperature gradient between the top and bottom anvils. White, Zr rich spots, present in the homogenized alloy [12] and in the alloy after RT deformation (Fig. 2), are not seen in the 1273 K deformed sample. Instead, characteristic bands at grain boundaries and inside the grains are formed (Fig. 6b). Higher magnification images (Fig. 6c and d), as well as EBSD analysis (Fig. 7), show that these bands consist of fine, recrystal lized grains and have a fine duplex structure consisting of a mixture of the second phase precipitates and transformed matrix. The second phase particles, which have a dark color on the BSE images (Fig. 6c and d), become larger and their volume fraction increases, as compared to the non deformed sample [12] or the sample deformed at room temperature (Fig. 2). EDS analysis indicates that, inside the bands, the matrix is enriched with Zr and second phase particles are depleted of Zr (Table 4). In the regions outside the deformation bands, where the second phase particles are not detected, the non transformed matrix has a composition that is close to the average alloy composition. EBSD analysis indicates that both the matrix and second phase particles have BCC crystal structures, and the particles have the same crystal lographic orientations as the respective matrix grains (Fig. 7). The presence of internal stresses inside the grains, especially near grain boundaries, is recognized by continuous change in the orientation of the crystal lattice (Fig. 7d).

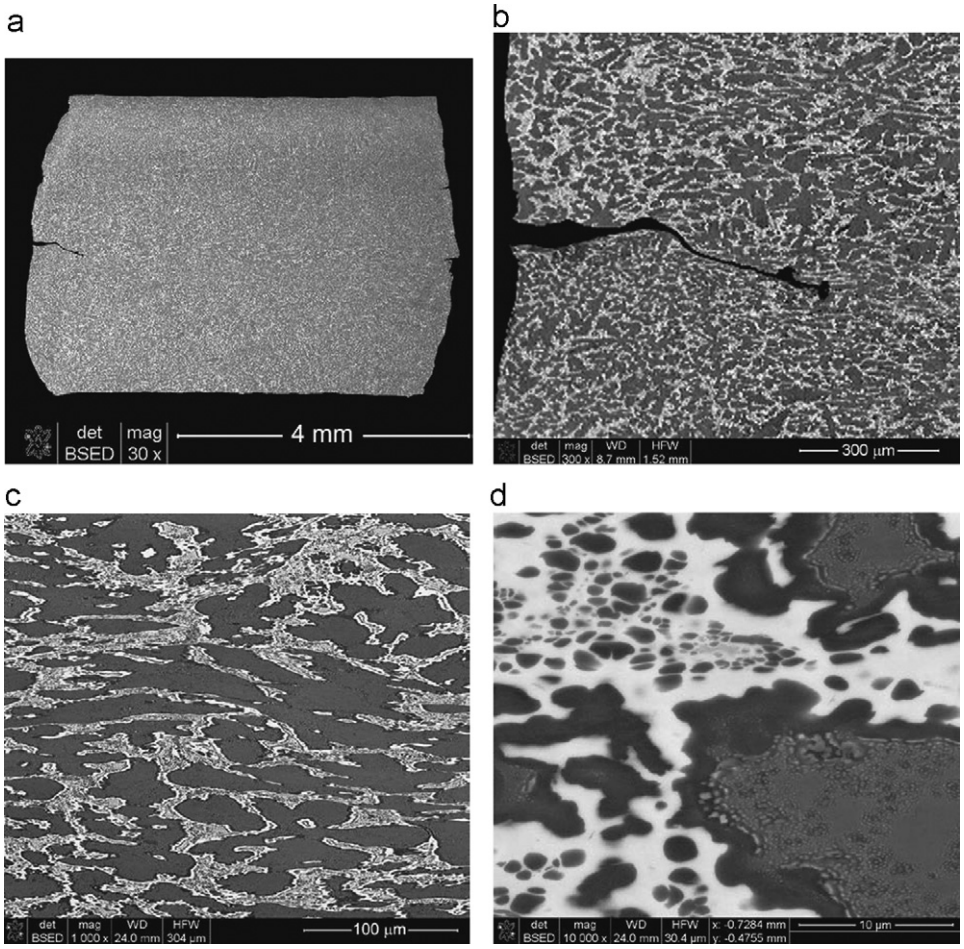

Fig. 3. The microstructure of the $NbTiV_2Zr$ alloy sample after 50% compression deformation at room temperature. (a) Overall sample cross-section; (b) a magnified image of the crack and surrounding area at the left side edge of the specimen; (c) deformed matrix and particles; and (d) a higher magnification image indicating that all three phases presented in the alloy are ductile.

Table 5
Chemical composition of the $NbTiV_2Zr$ alloy constituents after compression at 298 K and 1273 K.

Condition	Deformed at 298 K				Deformed at 1273 K			
At%	Nb	Ti	V	Zr	Nb	Ti	V	Zr
White regions	21.1	18.8	10.9	49.2	22.2	22.6	10.5	44.7
Gray regions	24.5	20.0	41.1	14.4	19.9	8.9	43.6	27.6
Dark regions	23.7	19.6	47.8	8.9	25.7	21.2	45.4	7.6

The microstructure of the $NbTiV_2Zr$ alloy after 50% compression deformation at 1273 K is shown in Fig. 8. There is no particular directional texture for the constituent phases, which may indicate that continuous recrystallization occurred during deformation or that the material had only one BCC phase at 1273 K while other phases formed during cooling after deformation. The microstructure consists of (i) large, white color particles fragmented in fine grains and gray and dark color equiaxed particles (Fig. 8a and b), (ii) fine elongated precipitates of white and gray color located in the regions between the white particles (Fig. 8b and c) and (iii) dark particles/areas located between the elongated precipitates and near the white particles (Fig. 8b and c). EDS analysis confirms that the white, gray and dark constituents have different concentrations of the alloying elements (Table 5). In particular, the white particles are depleted of V and enriched with Zr, dark regions/particles are depleted of Zr and enriched with V, and gray particles are depleted with Ti. The analysis indicates that the compositions of the white and dark regions in the deformed at 1273 K sample are similar to the compositions of the respective regions in the non deformed alloy, while the gray regions become enriched with Zr and depleted of Ti after the deformation (Table 5). EBSD analysis shows that, in spite of different compositions, all three constituents have BCC crystal structures.

Fig. 9 and Fig. 10 illustrate microstructures of the CrNbTiZr and CrNbTiVZr alloys, respectively, after 50% compression deformation at 1273 K. Before deformation, in the homogenized condition, these alloys contain two phases, a disordered BCC phase and an ordered Laves phase with the FCC crystal structure. The volume fraction of the Laves phase is 35 and 61% in CrNbTiZr and CrNbTiVZr, respectively. After the high temperature deformation, the two phase microstructure is retained, however, the interfaces between the phases are more rounded, the BCC phase particles become recrystallized and large Laves particles (especially in CrNbTiVZr) become twinned. No preferred orientation of the particles relative to the compression direction is identified. EDS analysis shows that the Laves phase is enriched with Cr, while the BCC phase is enriched with Ti and Nb in these alloys (Table 6 and Table 7). The phase chemical compositions are similar to those in the respective alloys before deformation.

3.2.3. Effect of deformation at 1273 K on the phase composition of the alloys

X ray diffraction patterns of the studied alloys before and after deformation at 1273 K are shown in Figs. 11 14. While only one

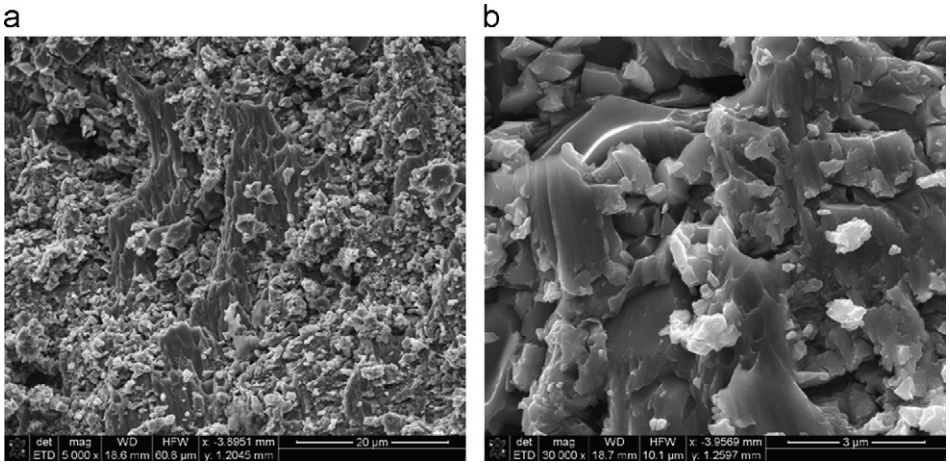

Fig. 4. The microstructure of the fracture surface of the CrNbTiZr alloy. The compression fracture strain is 6%. (a) A low magnification image showing the fracture surface decorated with fine particles produced during the fracture event leading to explosion-like specimen fragmentation; (b) a higher magnification image showing plastically deformed dimples and the pulverized fragments.

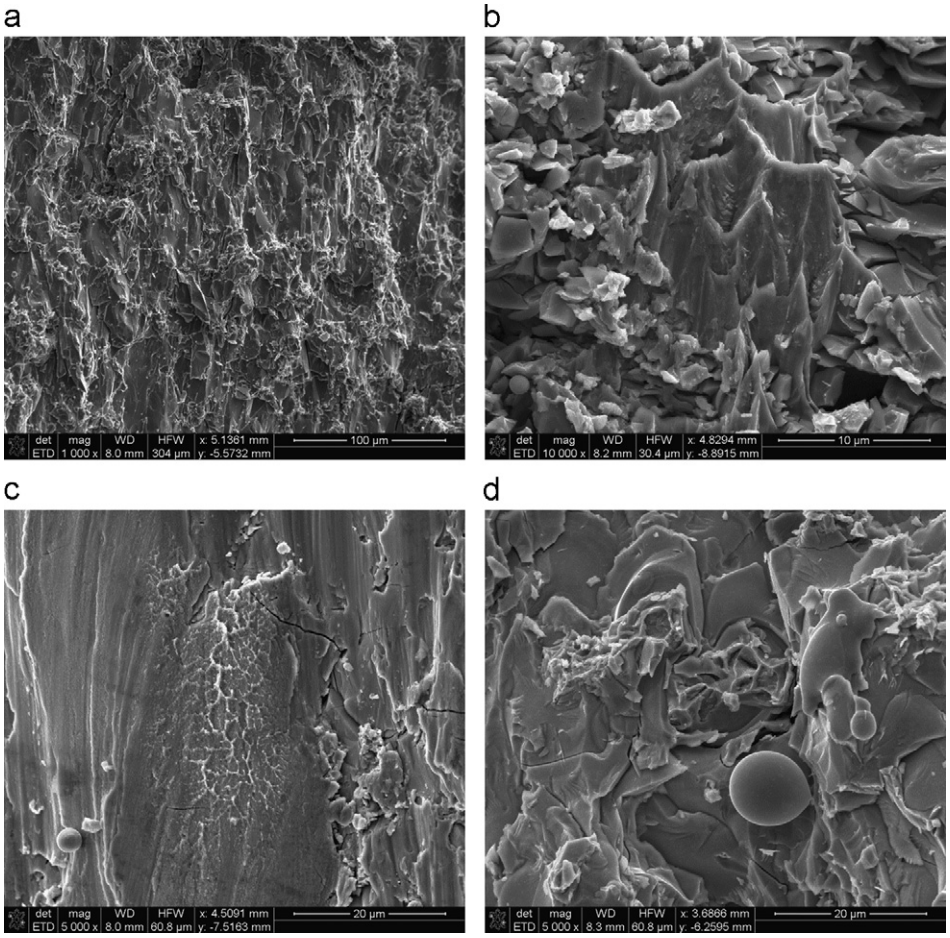

Fig. 5. The fracture surface of the CrNbVTiZr alloy fractured at room temperature during compression deformation. The compression fracture strain is 3%. (a) Low magnification and (b) higher magnification images illustrating a mixed type of fracture consisting of plastically deformed dimples and brittle fragmented particles. (c,d) Regions on the fracture surface of the CrNbTiVZr alloy sample indicating local sample melting during fracture.

BCC phase is recognized in the NbTiVZr before deformation, three BCC phases are clearly seen after deformation (Fig. 11). The lattice parameter of the matrix phase slightly decreases from $a_1=$ 332.5 pm to $a_1=331.8$ pm, and the two new phases have the lattice parameters of $a_2=345.4$ pm and $a_3=323.9$ pm, respec tively. The development of diffraction peaks from the additional phases is definitely due to the increased volume fraction of these phases, as well as larger dimensions of the second phase parti cles. It is likely that the new phases form during decomposition of the matrix phase within the deformation bands. Based on ele mental lattice constants of the BCC crystals [6,8], the phase with a larger lattice parameter ($a_2=345.4$ pm) is likely enriched with

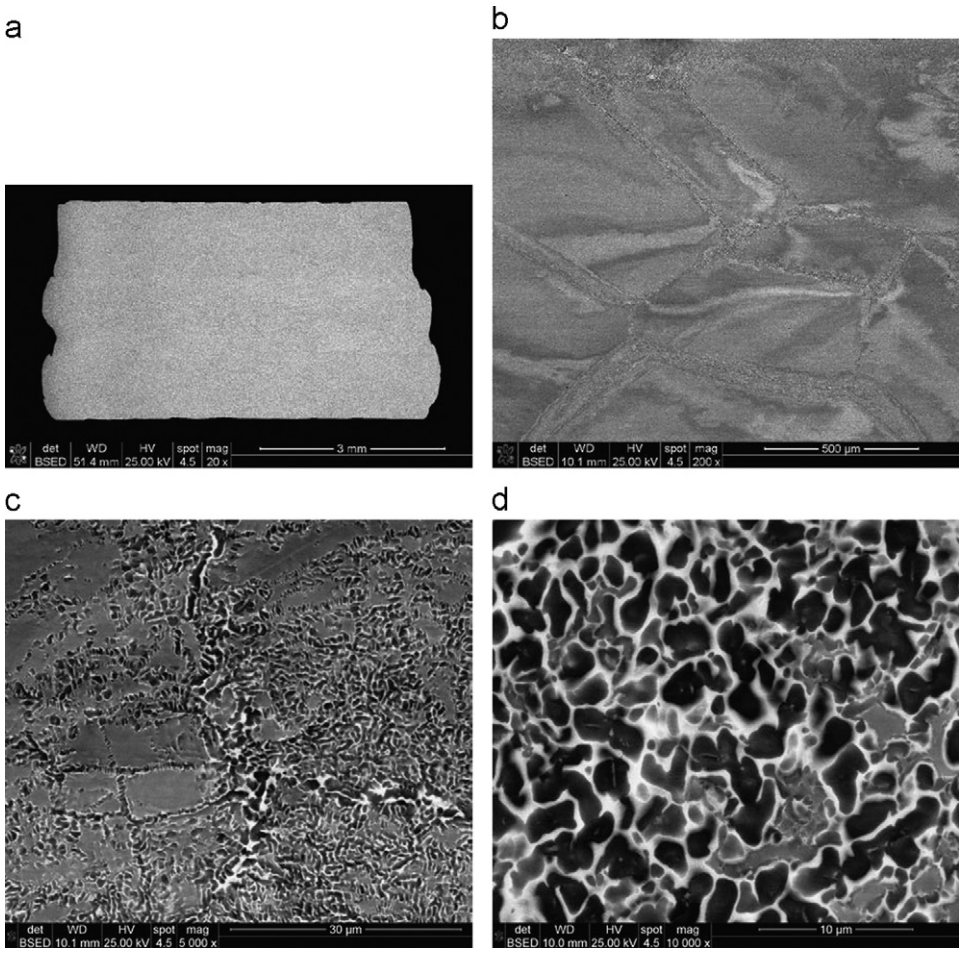

Fig. 6. The microstructure of the NbTiVZr alloy after 50% compression deformation at T 1273 K: (a) a longitudinal cross-section of the deformed sample, (b) grains with heavily deformed bands along grain boundaries, (c,d) precipitated particles inside the bands.

Zr and is represented by white particles (transformed matrix) in Fig. 6, while the phase with the smaller lattice parameter (a_3=323.9 pm) is enriched with V (see Table 5) and is represented by dark particles. The BCC1 phase, with the lattice parameter a_3=331.8 pm, is a non transformed high temperature phase, which is in equilibrium above 1000 K [12]. The secondary phase dark particles are also present in the non deformed alloy, but they are much finer and are precipitated at subgrain boundaries and at individual dislocations in the form of characteristic chains [12]. It has been therefore suggested that these particles are formed by heterogeneous nucleation. The fact that these particles are abun dant inside the deformation bands in the deformed sample supports the mechanism of heterogeneous nucleation. Moreover, it is likely that the phase transformation occurred not during the high temperature deformation but during cooling after deforma tion and the high number density of dislocations in the deformed sample facilitates and accelerates this transformation. Indeed, thermodynamic simulation of the equilibrium phase diagram for NbTiVZr conducted in previous work [12] predicts only one BCC phase above 1000 K. The volume fraction of the second BCC phase, which is enriched with Nb and V, is predicted to increase very rapidly from 0 to 36% with a decrease in the temperature from ~1000 K to 873 K, thus causing the remaining matrix phase to become enriched with Zr and depleted of V.

The X ray diffraction pattern of the homogenized $NbTiV_2Zr$ shows three BCC phases, with lattice parameters a_1=317.4 pm, a_2=345.8 pm and a_3=323.5 pm. After deformation at 1273 K, the diffraction peaks from only two phases, BCC1 and BCC2, with lattice parameters of a_1=317.9 pm and a_2=343.8 pm are present (Fig. 12). However, SEM/EDS analysis still clearly indicates the presence of three constituents with distinct compositions (Table 5). The different diffraction patterns of the homogenized and high temperature deformed alloy samples can be explained by a more complete transformation occurring after deformation facilitated by heterogeneous nucleation of the low temperature BCC1 phase on deformation induced defects (e.g. dislocations, subgrain boundaries, points defects, etc.). In accordance with the equilibrium phase diagram modeled in [12], the $NbTiV_2Zr$ has a single phase BCC structure above 1116 K, which partially trans forms to a low temperature BCC phase (enriched with Nb and V) below this temperature. At temperatures of 960 1030 K, these phases are present in almost equal volume fractions, and at 873 K the volume fraction of the low temperature BCC phase becomes about 52%. Therefore, it is anticipated that during deformation at 1273 K the $NbTiV_2Zr$ had a single phase structure, and the multi phase structure shown in Fig. 8 formed during cooling after deformation. Due to slow diffusion kinetics of the alloying elements, equilibrium conditions are probably not reached during the continuous cooling process and the structure/phases typical of the high temperatures are quenched in. Because the deformed alloy has more crystal defects for heterogeneous nucleation of the low temperature phase than the annealed alloy, the transforma tion in the former condition should occur more extensively and in larger regions than in the latter (homogenized) condition. The presence of diffraction peaks from three BCC phases in the homogenized condition thus may indicate that some regions

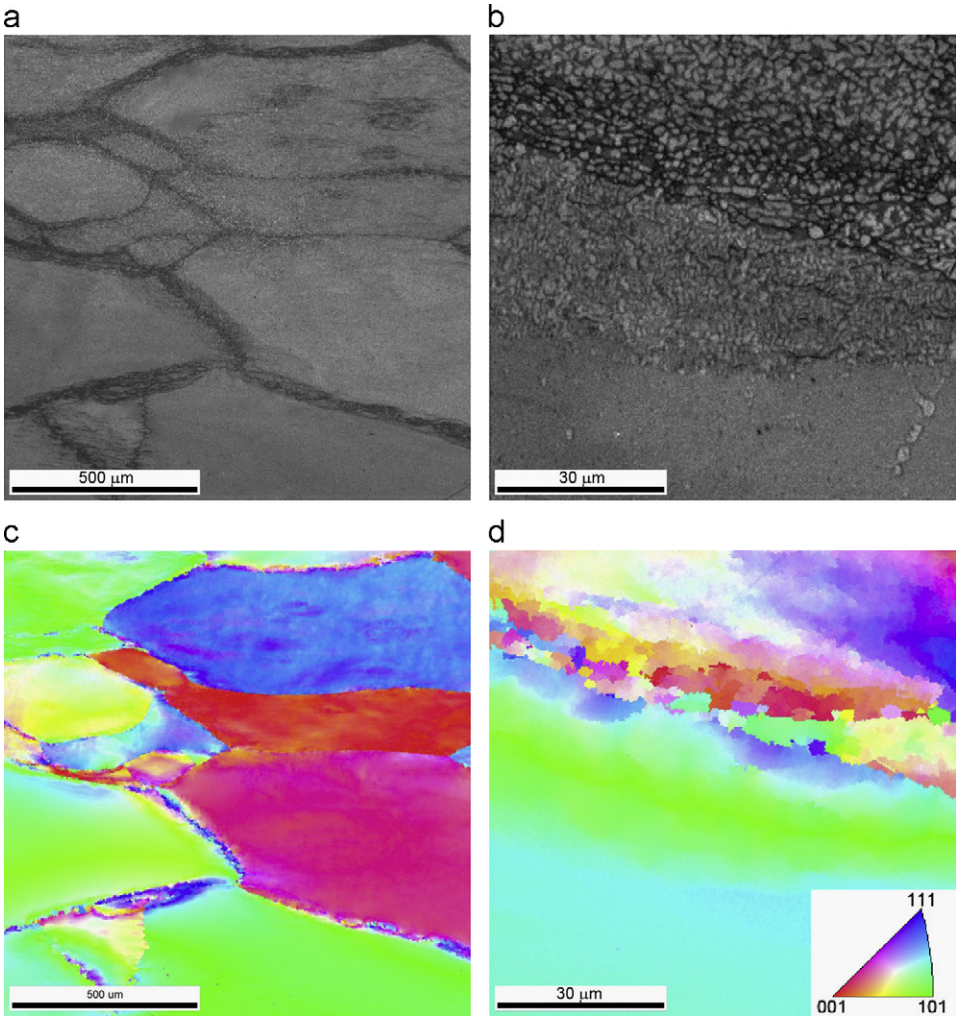

Fig. 7. EBSD/SEM images of (a) deformed grains, (b) grain boundary area, and (c,d) respective inverse pole figure images showing unique crystallographic orientations of (c) original large grains and (c,d) new fine grains formed at grain boundaries of the deformed grains.

of the sample contain a non transformed high temperature BCC phase (which is represented in Fig. 12a as BCC3, with $a_3 =$ 323.5 pm and which composition is closer to the composition of the alloy), while other regions experience more complete phase transformation, resulting in a considerable change in the chem istry (and the lattice parameter) of the high temperature phase. As the Zr rich phase should have larger lattice parameter than the V rich one, one may suggest that the BCC1 phase ($a_1 = 317.4$ pm) is enriched with V and represent dark regions, while the BCC2 phase ($a_2 = 345.8$ pm) is enriched with Zr and represent white particles in Fig. 8. On the other hand, due to more complete phase transformation during cooling, the deformed alloy has a much smaller volume fraction of the non transformed high tempera ture phase and thus the BCC3 phase is not seen or it is shielded by diffraction peaks from the BCC1 phase (Fig. 12b).

The X ray diffraction patterns of the Cr containing alloys, CrNbTiZr and CrNbTiVZr, are almost not affected by high tem perature deformation (see Fig. 13 and Fig. 14). The lattice para meters of the BCC and Laves phases are almost the same as in the non deformed condition. The chemical compositions of these phases in the deformed and non deformed conditions are also almost identical in the respective alloys (see Table 6 and Table 7). This observation is in agreement with the phase diagrams recently calculated for these alloys [12]. Indeed, according to these diagrams, the Laves phase is present at temperatures below 1636 K and 1546 K for the CrNbTiZr and CrNbTiVZr, respectively, and at $T \leq 1273$ K the volume fraction of this phase is very weakly temperature dependent. On the other hand, at temperatures between 1473 K (annealing temperature) and 1273 K (deformation temperature) diffusion of the alloying elements is expected to occur quickly enough to accommodate equilibrium conditions, thus providing similar phase compositions of the annealed and deformed alloy samples.

4. Discussion

4.1. Deformation behavior at room temperature

The produced refractory multi principal element alloys have high yield strength and hardness at room temperature. NbTiVZr and $NbTiV_2Zr$ consist of disordered BCC phases with rather large grain sizes (about 500 600 μm) and their high hardness and strength, as well as their strong tendency to deformation strength ening (Fig. 1), are evidently due to solid solution like strengthening [6,7]. The high tendency to deformation strengthening and the absence of brittle intermetallic phases are probably the main reasons of good ductility of these two alloys. In spite of having a more complex and refined microstructure consisting of three BCC phases, the $NbTiV_2Zr$ alloy has smaller yield strength and hardness at room temperature than the single phase NbTiVZr (see Table 2 and Table 3). This observation can be explained by different

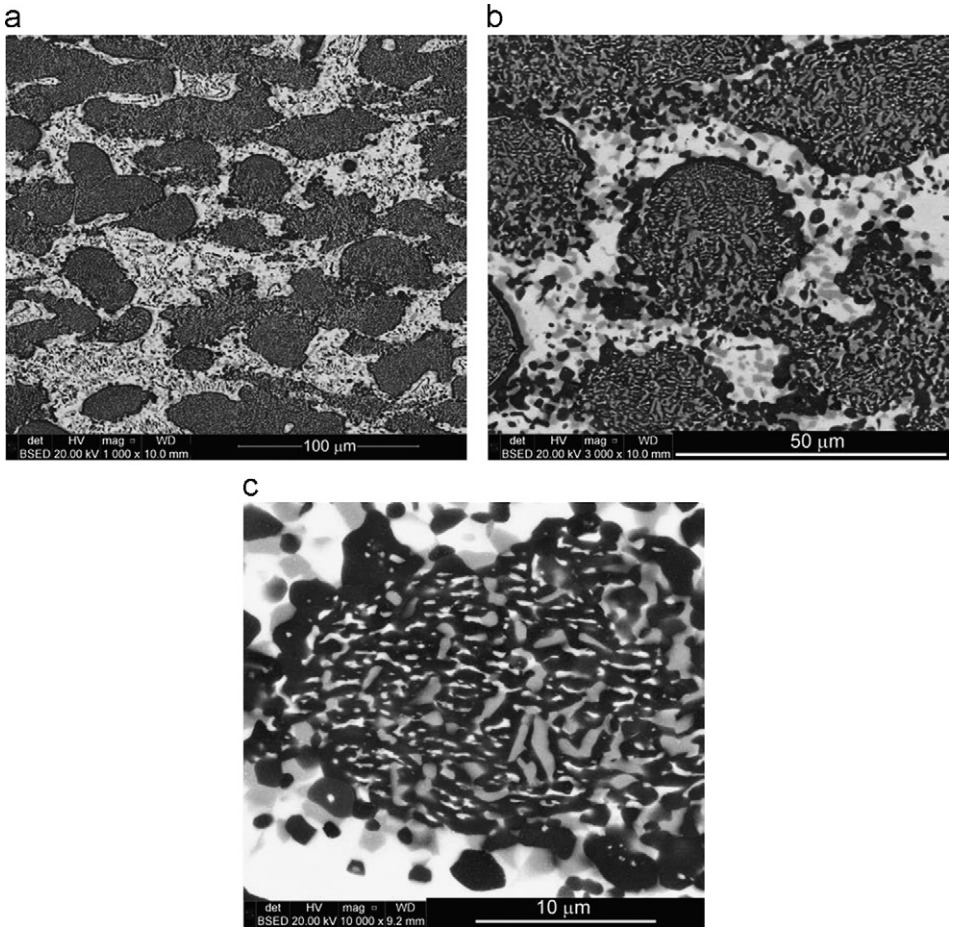

Fig. 8. The microstructure of the $NbTiV_2Zr$ alloy after 50% compression deformation at T 1273 K. Different magnification images illustrate coarse and fine microstructure features, as well as the morphologies of the three phases presented in the sample.

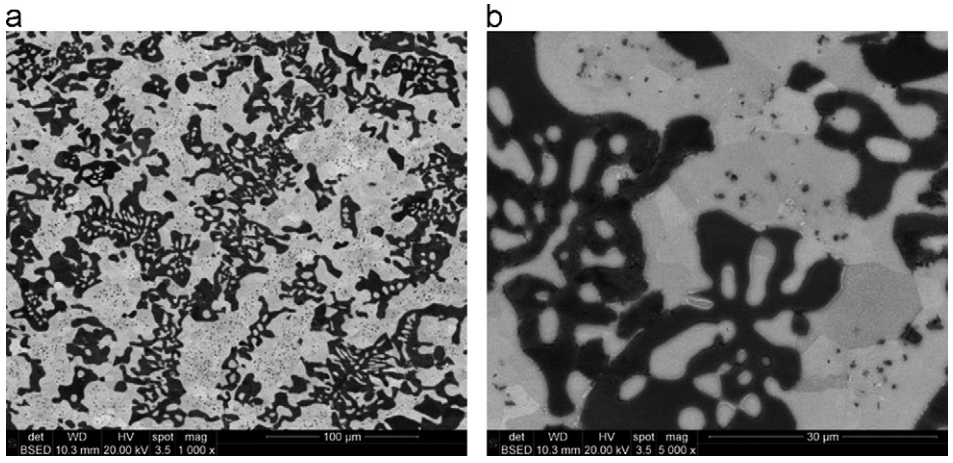

Fig. 9. The microstructure of the CrNbTiZr alloy after 50% compression deformation at T 1273 K.

non equilibrium conditions of the BCC phases and thus their different super saturation with the alloying elements in these two alloys. Indeed, the BCC phase presented in NbTiVZr is a non equilibrium, non transformed high temperature phase, quenched from the high temperature single phase BCC region during cooling after homogenized annealing. This phase has almost the same composition as the average composition of the alloy and thus it is highly super saturated with the alloying elements. On the other hand, two of the three BCC phases present in $NbTiV_2Zr$ at a total volume fraction of ~80% [12] (identified as BCC1and BCC2 in Fig. 12a) are the results of decomposition of the high temperature BCC phase (BCC3) and thus these phases are less super saturated than the quenched high temperature phase. Therefore, the NbTiVZr alloy should have a stronger solid solution strengthening effect than $NbTiV_2Zr$. The presence of very fine precipitates can also add to the strengthening of the NbTiVZr alloy.

In spite of higher strength than the two other alloys, the Cr containing alloys, CrNbTiZr and CrNbTiVZr, show low ductility at

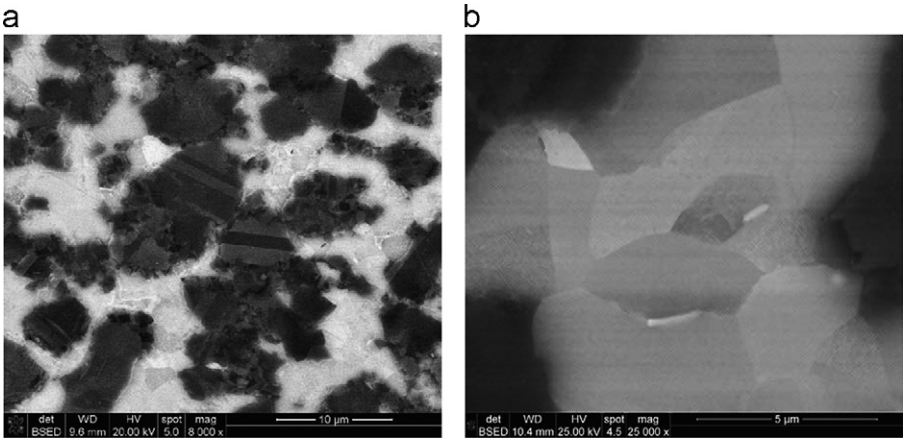

Fig. 10. The microstructure of the CrNbTiVZr alloy after 50% compression deformation at T 1273 K. (a) A duplex equiaxed structure and (b) recrystallized grains inside the matrix phase.

Table 6
Chemical composition of the CrNbTiZr alloy constituents after homogenization and after compression at 1273 K.

Condition	Homogenized				Deformed			
At%	Cr	Nb	Ti	Zr	Cr	Nb	Ti	Zr
Bright regions	7.9	34.6	31.4	26.1	4.7	33.8	35.3	26.2
Dark regions	51.5	15.8	12.1	20.6	53.7	14.1	12.6	19.6

Table 7
Chemical composition of the CrNbTiVZr alloy constituents after homogenization and after compression at 1273 K.

Condition	Homogenized					Deformed				
At%	Cr	Nb	Ti	V	Zr	Cr	Nb	Ti	V	Zr
Bright regions	4.1	31.6	33.1	12.8	18.4	3.2	29.1	36.8	12.9	18.0
Dark regions	29.4	16.1	9.7	22.2	22.7	31.7	13.9	9.7	23.7	21.0

room temperature. Both an increased yield strength and considerably reduced ductility of these alloys are caused by a strong but brittle Laves phase.

4.2. High temperature deformation behavior

During deformation at high temperatures, 1073 K and 1273 K, all four alloys are ductile and show a steady state plastic flow at almost constant flow stress, which decreases with an increase in temperature and depends on the alloy composition (see Fig. 1). At these temperatures, the $NbTiV_2Zr$ alloy becomes stronger than NbTiVZr and the Cr containing alloys, CrNbTiZr and CrNbTiVZr, are more than twice stronger than the Cr free alloys (see Table 2). Such different behavior of the alloys is likely due to their different phase compositions in this temperature range. According to equilibrium phase diagrams [12], the NbTiVZr and $NbTiV_2Zr$ alloys have a single equilibrium BCC phase during deformation at 1073 K and 1273 K, while the two Cr containing alloys retain their two phase, BCC and Laves, structure, with very weak temperature dependence of the volume fraction of the Laves phase. Therefore, the yield and steady state flow stresses of the NbTiVZr and $NbTiV_2Zr$ alloys are controlled by solid solution like strengthening of the equilibrium BCC phase. Higher concentration of V, which has the smallest atomic radius among the alloying elements, likely results in larger distortion of the BCC crystal lattice [6], which explains higher strength of the $NbTiV_2Zr$ alloy relative to that of NbTiVZr. The high temperature strength of the Cr containing alloys is obviously controlled by the strength of the Laves phase, thus almost twice larger volume fraction of the Laves phase results in a similar increase in the high temperature yield strength of the CrNbTiVZr alloy, relative to CrNbTiZr (see Table 2).

4.3. Comparison with other alloys

Fig. 15 shows the temperature dependences of the specific yield strength (SYS) of the studied alloys. The SYS of a HfNbTaTiZr HEA [7] and two Ni superalloys, Inconel 718 [16] and Haynes 230 [17] are also shown for comparison. At room temperature, the SYS values of all the studied alloys are more than 3 times higher than the SYS of Haynes 230 and more than 1.5 times higher than the SYS of HfNbTaTiZr. The RT SYS of the $NbTiV_2Zr$ is the same as while those of NbTiVZr, CrNbTiZr and CrNbTiVZr are higher than the SYS of Inconel 718. At 873 K, the studied alloys are stronger than Haynes 230 and HfNbTaTiZr, while the CrNbTiZr and CrNbTiVZr are also stronger than Inconel 718. The SYS of NbTiVZr is the same as, while that of $NbTiV_2Zr$ is lower than the SYS of Inconel 718 at 873 K. At 1073 K, the SYS of NbTiVZr, $NbTiV_2Zr$ and CrNbTiZr are smaller than SYS of Inconel 718 and HfNbTaTiZr, but are equal or higher than the SYS of Haynes 230. At 1273 K, the SYS of NbTiVZr, $NbTiV_2Zr$ and CrNbTiZr are smaller than SYS of HfNbTaTiZr, but are equal or higher than the SYS of the two Ni superalloys. The SYS values of the CrNbTiVZr at 1073 K and 1273 K are considerably higher than the respective SYS values of the referenced alloys. These results indicate that, among the four refractory alloys studied in this work, the CrNbTiVZr alloy has the most attractive set of properties, such as considerably improved elevated temperature strength and reduced density, relative to Ni superalloys. The Laves phase is likely responsible for the elevated temperature strength of the CrNbTiVZr alloy, but it is also responsible for the reduced room temperature ductility. The limited room temperature ductility is a major obstacle for structural use of this alloy. However, it is expected that the limited ductility is not an intrinsic property of the Cr containing alloys, and depends sensitively on the microstructure, especially the size and distribution of the Laves phase. The Laves phase in this alloy can be dissolved above about 1500 1700 K [12], and this offers the possibility of microstructure and property control through dissolu tion and controlled precipitation of the Laves phase in the form of nano or submicron size particles. This work thus suggests a reasoned approach for developing high entropy alloys with both solid solution and ordered phases as candidate high temperature structural materials. Such studies are recommended for future work.

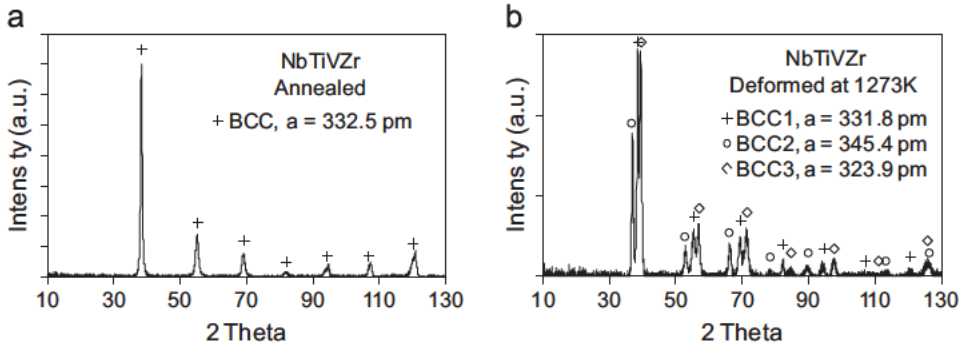

Fig. 11. X-ray diffraction patterns of the NbTiVZr alloy after (a) homogenization annealing at 1473 K and (b) compression deformation at 1273 K.

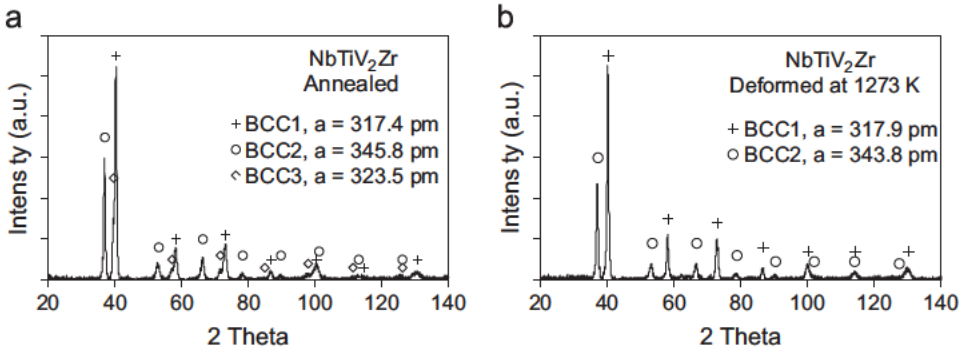

Fig. 12. X-ray diffraction patterns of the $NbTiV_2Zr$ alloy after (a) homogenization annealing at 1473 K and (b) compression deformation at 1273 K.

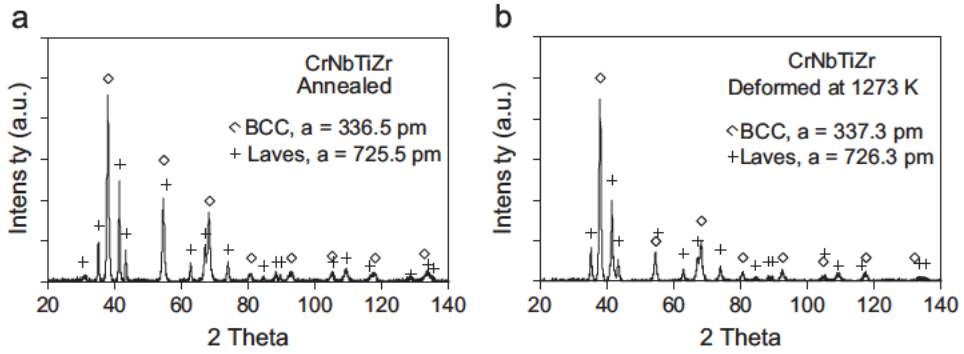

Fig. 13. X-ray diffraction patterns of the CrNbTiZr alloy after (a) homogenization annealing at 1473 K and (b) compression deformation at 1273 K.

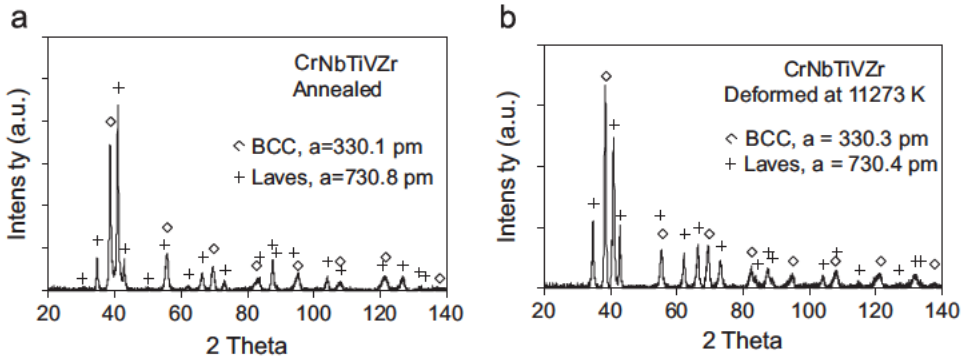

Fig. 14. X-ray diffraction patterns of the CrNbTiVZr alloy after (a) homogenization annealing at 1473 K and (b) compression deformation at 1273 K.

5. Conclusions

A new alloy development strategy based on stabilizing the solid solution of four or more principal elements has been used to produce four new alloys. Properties of these materials were measured using compression tests in order to assess which alloys warrant further study.

1. New refractory multi principal element alloys, NbTiVZr, $NbTiV_2Zr$, CrNbTiZr, and CrNbTiVZr, have densities of 6.52,

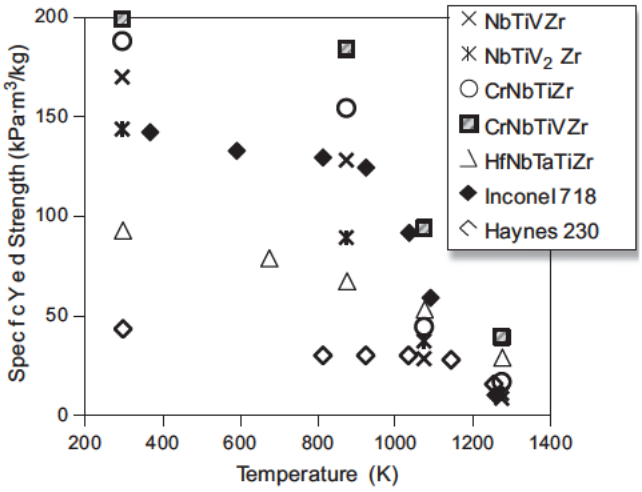

Fig. 15. The temperature dependence of the specific yield strength of the NbTiVZr, $NbTiV_2Zr$, CrNbTiZr and CrNbTiVZr alloys studied in this work in comparison with that of a HfNbTaTiZr high entropy alloy [7] and Inconel 718 [16] and Haynes 230 [17] superalloys.

6.34, 6.67 and 6.57 g/cm^3, respectively. After homogenization at 1473 K for 24 h and slow cooling at a rate of 10 K/min, the NbTiVZr is essentially single phase BCC crystal structure with small amount of submicron sized particles precipitated at grain boundaries and dislocations. The composition of the BCC phase is close to the composition of the alloy. The $NbTiV_2Zr$ contains three disordered BCC phases, one of which has the composition close to the composition of the alloy, another is enriched with Zr and the third is enriched with V. The CrNbTiZr and CrNbTiVZr alloys consist of a disordered BCC phase and an ordered Laves phase, with the volume fraction of the latter of 35% and 61%, respectively. The Laves phase is rich with Cr in CrNbTiZr and with Cr and V in CrNbTiVZr, while the BCC phase is enriched with Nb and Ti in both Cr containing alloys.

2. The compression properties of the NbTiVZr, $NbTiV_2Zr$, CrNbTIZr, and CrNbTiVZr alloys were determined in the temperature range from 298 K to 1273 K. The NbTiVZr and $NbTiV_2Zr$ alloys showed good compressive ductility at all studied temperatures while the Cr containing alloys showed brittle to ductile transi tion occurring somewhere between RT and 873 K.
3. Strong work hardening was observed in the NbTiVZr and $NbTiV_2Zr$ alloys during deformation at room temperature. The alloys had yield strengths of 1105 MPa and 918 MPa, respec tively, and their strength continuously increased, exceeding 2000 MPa after ~40% compression strain.
4. The CrNbTiZr and CrNbTiVZr alloys showed high yield strength (1260 MPa and 1298 MPa, respectively) but low ductility (6% and 3% compression strain, respectively, before the fracture) at room temperature. Cleavage fracture of Laves phase particles and ductile fracture of the BCC phase was observed in these alloys. The fracture of these alloys was associated with extensive material fragmentation and local heating beyond the melting temperature.
5. Strain softening and steady state flow were typical during compression deformation of these alloys at temperatures above 873 K. In these conditions, the alloys survived 50% compression strain without fracture and their yield strength continuously decreased with an increase in temperature. During deformation at 1273 K, the NbTiVZr, $NbTiV_2Zr$, CrNbTIZr, and CrNbTiVZr alloys showed yield strengths of 58 MPa, 72 MPa, 115 MPa and 259 MPa, respectively.
6. During deformation at 1273 K, the NbTiVZr and $NbTiV_2Zr$ alloys had a single phase BCC structure. After deformation at 1273 K followed by cooling to room temperature, the phase compositions of the NbTiVZr and $NbTiV_2Zr$ alloys noticeably changed relative to the respective homogenized conditions. In addition to the matrix phase, two additional BCC phases were observed in NbTiVZr, predominantly inside the deformation bands. In $NbTiV_2Zr$, the volume fraction of one of the three BCC phases observed after homogenization treatment considerably reduced after deformation. It is suggested that the high density of dislocations and subgrain boundaries in the deformed alloys facilitates transformation of the high temperature BCC phase into the low temperature BCC phase during cooling after deformation. The results indicate that the phases present in these two alloys at room temperature are likely metastable phases, which are quenched from higher temperatures due to slow diffusion kinetics of the alloying elements.
7. During deformation at 1273 K, the CrNbTIZr, and CrNbTiVZr alloys retained their two phase (BCC plus Laves) structure and their phase compositions were unaffected by deformation. The high temperature deformation resulted in formation of new recrystallized grains inside the BCC phase and deformation twins inside large Laves phase particles.
8. The CrNbTiVZr alloy showed the most attractive properties, such as considerably improved elevated temperature strength, reduced density and much higher melting point, as compared to three other high entropy alloys and referenced Ni super alloys (In718 and Haynes 230). A microstructural approach to improve the limited room temperature ductility is suggested via dissolution and controlled precipitation of the strengthen ing Laves phase.

Acknowledgments

This work was supported through the Air Force Research Labora tory Director's fund and through the Air Force on site contract no. FA8650 10 D 5226 conducted by UES, Inc., Dayton, Ohio.

References

[1] J.-W. Yeh, S.-K. Chen, S.-J. Lin, J.-Y. Gan, T.-S. Chin, T.–T. Shun, C.-H. Tsau, S.-Y. Chang, Adv. Eng. Mater. 6 (5) (2004) 299–303.
[2] J.-W. Yeh, Ann Chim., Sci. Mater. 31 (2006) 633–648.
[3] J.-W. Yeh, Y.-L. Chen, S.-J. Lin, S.-K. Chen, Mater. Sci. Forum 560 (2007) 1–9.
[4] O.N. Senkov, G.B. Wilks, D.B. Miracle, C.P. Chuang, P.K. Liaw, Intermetallics 18 (2010) 1758–1765.
[5] O.N. Senkov, G.B. Wilks, J.M. Scott, D.B. Miracle, Intermetallics 19 (2011) 698–706.
[6] O.N. Senkov, J.M. Scott, S.V. Senkova, D.B. Miracle, C.F. Woodward, J. Alloys Compd. 509 (2011) 6043–6048.
[7] O.N. Senkov, J.M. Scott, S.V. Senkova, F. Meisenkothen, D.B. Miracle, C.F. Woodward, J. Mater. Sci. 47 (2012) 4062–4074.
[8] O.N. Senkov, C.F. Woodward, Mater. Sci. Eng. A 529 (2011) 311–320.
[9] O.N. Senkov, S.V. Senkova, D.M. Dimiduk, C. Woodward, D.B. Miracle, J. Mater. Sci. 47 (2012) 6522–6534.
[10] Y. Zhang, Y.J. Zhou, J.P. Lin, G.L. Chen, P.K. Liaw, Adv. Eng. Mater. 10 (6) (2008) 534–538.
[11] Y. Zhang, X. Yang, P.K. Liaw, JOM 64 (7) (2012) 830–838.
[12] O.N. Senkov, S.V. Senkova, D.B. Miracle, C. Woodward, Low-density, refrac- tory multi-principal element alloys of Cr–Nb–Ti–V–Zr system: microstruc- ture and phase analysis. Acta Mater. http://dx.doi.org/10.1016/j.actamat. 2012.11.032, in press.
[13] J. Eckert, G. He, Z.F. Zhang, W. Löser, J. Metastable Nanocryst. Mater. 20–21 (2004) 357–365.
[14] H.L. Min, D.J. Sordelet, Appl. Phys. Lett. 88 (2006) 261902/1–3.
[15] L.S. Vasilev, Russ. Met. 1 (2008) 66–75.
[16] Inconel® Alloy 718, 〈http://www.specialmetals.com/documents/Inconel alloy 718.pdf〉.
[17] Haynes® 230® Alloy, 〈www.haynesintl.com/pdf/h3060.pdf〉.